Supplemental Material
Probing a dissipative phase transition via dynamical optical hysteresis

S.R.K. Rodriguez,[1] W. Casteels,[2] F. Storme,[2] N. Carlon Zambon,[1] I. Sagnes,[1]
L. Le Gratiet,[1] E. Galopin,[1] A. Lemaître,[1] A. Amo,[1] C. Ciuti,[2] and J. Bloch[1]

[1]*Centre de Nanosciences et de Nanotechnologies, CNRS, Univ. Paris-Sud, Université Paris-Saclay, C2N—Marcoussis, 91460 Marcoussis, France*
[2]*Laboratoire Matériaux et Phénomènes Quantiques, Université Paris Diderot, Sorbonne Paris Cité and CNRS, UMR 7162, 75205 Paris Cedex 13, France*

(Dated: June 1, 2017)

Sample details

The planar cavity was grown by molecular beam epitaxy and comprises a GaAs λ cavity between two $Ga_{0.9}Al_{0.1}As/Ga_{0.05}Al_{0.95}As$ distributed Bragg reflectors with 26 and 30 pairs of layers at the top and bottom, respectively. One 80 Å-wide $In_{0.04}Ga_{0.96}As$ quantum well is positioned at the center of the cavity. A Rabi splitting of 3.4 meV results from strong exciton-photon coupling. The three rectangular micropillars (all having 2:1 aspect ratio) were fabricated by electron beam lithography and dry etching of the planar cavity. With reference to the labels in Fig. 4(a) of the main manuscript, the cross-sectional area A_c of the micropillars are: $A_c = 6\ \mu\mathrm{m}^2$ for cavity 1, $A_c = 8\ \mu\mathrm{m}^2$ for cavity 2, and $A_c = 29\ \mu\mathrm{m}^2$ for cavity 3.

Measurement details

The driving laser is a tunable MSquare Ti:Sapphire oscillator with a linewidth below 10 MHz. The laser frequency is locked with an accuracy of 0.1 pm. Given the typical values of γ and $\hbar\omega_0$ (see above), this translates to an uncertainty in Δ/γ on the order of ± 0.01. The excitation and collection objectives have a numerical aperture of 0.5 and 0.4, respectively. For all three cavities the excitation laser beam is linearly polarized parallel to the long axis of the rectangular micropillars, thereby probing the lowest energy mode. For the cavity under study in all figures of the main text, the lowest energy mode for the orthogonal polarization (along the short axis) is $\sim 5\gamma$ higher in energy, while co-polarized higher energy states are several tens of γ away. Thus, the single mode approximation holds reasonably well.

To verify that our dynamic hysteresis measurements were shot-noise limited, we analyzed the power spectral density of the driving laser. The laser beam passed through our entire optical setup to reproduce the experimental conditions of the dynamic hysteresis measurements. At low frequencies (1- 50 Hz), where various fluctuations are significant, Fig. S1(a) shows that the noise amplitude scales linearly with the total power. In contrast, at higher frequencies Fig. S1(b) shows that the noise amplitude scales with the square root of the total power, as expected for shot noise. We also observed a frequency-independent noise power spectral density (characteristic of shot noise) in the frequency range of Fig. S1(b). In addition, we note that the power in the modulated signal of our dynamic hysteresis measurements exceeds the noise level by more than four orders of magnitude.

Noise sources Additional sources of noise (besides shot noise) could also induce switching between metastable states. For instance, in Ref. 1 a large amount of noise was deliberately added to the driving laser to trigger switching between the two metastable states. In addition, noise could be generated within the cavity. For example, the intracavity polariton field could be subjected to fluctuations linked to acoustic phonon scattering or two photon absorption. In our experiments, phonon scattering can be excluded because kT is much smaller that the energy difference between the state we probe and the next confined polariton state. Fluctuations induced by two photon absorption can be ruled out considering the experiments reported in Fig.4(a). When probing smaller values of U/γ for fixed Δ/γ, the driving intensity at the critical point is larger. Stronger driving is expected to make two-photon absorption more relevant and thereby reduce the hysteresis area. However, the opposite behavior is observed and we can therefore neglect additional fluctuations induced within the cavity. Thus, we can safely consider that shot noise is the only relevant source of noise in our experiments.

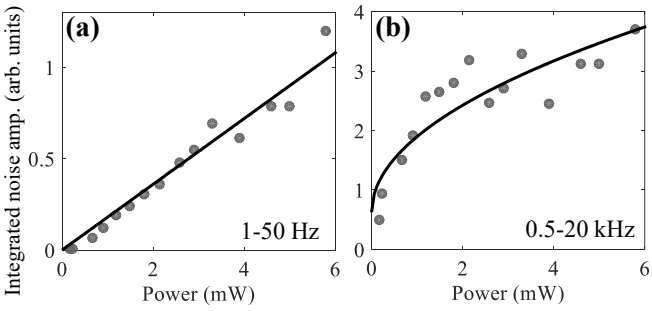

FIG. S1. Power-dependence of the noise amplitude in the driving laser integrated over the frequency range indicated in each panel. The black line in (a) is a linear fit, and the black line in (b) is a square root fit. The square root behavior at high frequencies is indicative of shot noise.

Retrieval of parameters

The mode frequency ω_0 and polariton loss rate γ of each micropillar were deduced by measuring the transmitted spectrum under weak driving ($< 1\mu$W), and fitting a Lorentzian lineshape as shown in Fig. 1(b) of the main manuscript. The polariton-polariton interaction energy U of each micropillar was estimated following the procedure described in detail in Ref. 2, and which we summarize below. To begin, we took the exciton-exciton interaction constant to be $g_{\rm exc} = 30\ \mu\text{eV}\cdot\mu\text{m}^2$. This value is consistent with theoretical predictions [3] and with our previous observations [2]. Next, we calculated the 2D polariton-polariton interaction constant as $U_{\rm 2D} = g_{\rm exc}|X|^4$, with $|X|^2$ the exciton fraction of the polariton admixture. To obtain the value of $|X|^2$ as a function of energy, we analyzed the exciton-polariton dispersion in an effectively 2D cavity adjacent to the micropillars in the wafer. In particular, we fitted the eigenvalues of a 2×2 Hamiltonian to the polariton dispersion, and obtained $|X|^2$ from the eigenvector associated with the lower polariton eigenvalue (energy). We then evaluated the value of $|X|^2$ at the energy of each micropillar mode to calculate $U_{\rm 2D}$. Finally, using the cross-sectional area of each micropillar A_c, we obtain $U = U_{\rm 2D}/A_c$.

The retrieved parameters are:

i) For the cavity under study in all figures of the main manuscript [cavity 2 in Fig. 4(a)], we have $\hbar\omega_0 = 1478.687 \pm 0.004$ meV, $\gamma = 31 \pm 2\mu eV$, $|X|^2 = 0.13$, and $U/\gamma = 2^{+8}_{-1.6}\cdot 10^{-3}$.

ii) For cavity 1 in Fig. 4(a) of the main manuscript, we have $\hbar\omega_0 = 1479.695 \pm 0.004$ meV, $\gamma = 31 \pm 3\mu eV$, $|X|^2 = 0.21$, and $U/\gamma = 1^{+4}_{-0.8}\cdot 10^{-2}$

iii) For cavity 3 in Fig. 4(a) of the main manuscript, we have $\hbar\omega_0 = 1472.752 \pm 0.004$ meV,$\gamma = 30 \pm 2\mu eV$, $|X|^2 = 0.02$, and $U/\gamma = 2^{+8}_{-1.6}\cdot 10^{-5}$.

Residence time measurements

In this section we explain how we measured the characteristic residence times which we compare with the tunneling times $\tau_{\rm tunn}$ in Fig. 1(d) of the main text. Essentially, we measured the cavity transmission at a fixed driving power as a function of time. We repeated such measurements for various powers and for several laser-cavity detunings Δ/γ. Figure S2 shows measurements at three representative powers for $\Delta/\gamma = 1.09 \pm 0.1$. The three panels display stochastic switching between two metastable states. Each metastable state is evidenced as a 'plateau' in the transmitted intensity.

Figure S2(a) shows that the system resides mostly in the state of lower photon density for a driving power slightly below the center of the bistability. In contrast, in Fig. S2(c) the system resides mostly in the state of higher photon density because the driving power is higher. In between those two cases, Fig. S2(b) shows that the system resides approximately (but not exactly) equal time on average in the high and low photon density states for a driving power close to the center of the bistability. As indicated in Fig. S2(b), we label the residence times in the lower state as $\tau_\downarrow$ and in the upper state as $\tau_\uparrow$.

Figure S3 shows a histogram of the residence times $\tau_\uparrow$ in the upper metastable state in Fig. S2(b). The dashed line in Fig. S3 is a least-squares fit of an exponential decay function to the the experimental data. From the fitted decay constant we extract a characteristic residence time of $\overline{\tau_\uparrow} = 4.7 \pm 0.5\ \mu$s. Good statistics were obtained by measuring the cavity transmission for times much longer than $\overline{\tau_\uparrow}$. In particular, we measured for a total time of 6 ms. A distribution similar to the one in Fig. S3 (not shown) was obtained for $\tau_\downarrow$. Moreover, this procedure was repeated for 10 different driving powers around the center of the bistability, for each detuning Δ/γ. For each trajectory we obtained the characteristic residence times $\overline{\tau_\downarrow}$ and $\overline{\tau_\uparrow}$, and we identified I_c as the driving power for which $\overline{\tau_\downarrow} = \overline{\tau_\uparrow}$. At exactly I_c, the system can be approximately described by two modes with inverse transition rate $\tau_{\rm tunn}$ [4]. Hence, $\overline{\tau}$ can be interpreted as $\tau_{\rm tunn}$ at I_c.

The retrieved values of $\overline{\tau}$ for several values of the laser-cavity detuning Δ/γ are shown on Fig. 1(d) of the main manuscript. Very good agreement between $\overline{\tau}$ and $\tau_{\rm tunn}$ is evidenced. The measurements were performed in the range of residence times corresponding to our dynamic hysteresis measurements, for which we previously showed that our setup is limited by shot-noise.

Mean-field calculation details

For the dynamic hysteresis calculations, we consider a triangular modulation of the drive intensity consisting of a linear sweep from I_0 to $I_0 + P_s$ followed by the reverse one from $I_0 + P_s$ back to I_0:

$$I(t) = I_0 + \frac{t}{t_s}P_s\theta(t_s - t) - \frac{t-2t_s}{t_s}P_s\theta(t - t_s), \quad (1)$$

Here, P_s is the range of the power sweep, t_s is the scanning time, and the effective sweep velocity is P_s/t_s. Introducing the sweep (1) in the equation of motion for the mean-field α (see main manuscript) with $t_s/P_s = 10^6/(5\gamma^3) = 2.1\cdot 10^{-5} s/\mu$W leads to the dynamic hysteresis presented in Fig. 2(d) of the main manuscript.

Scaling Analysis

In general, a master equation can be defined in terms of its Liouvillian superoperator $\hat{\mathcal{L}}$, namely $\partial_t\hat{\rho} = \hat{\mathcal{L}}\hat{\rho}$. The Liouvillian superoperator has a complex spectrum of eigenvalues λ. Their imaginary part has the meaning of an excitation frequency, while their real part determines the dissipation rate. The steady-state density matrix $\hat{\rho}_{ss}$ corresponds to the eigenvector of $\hat{\mathcal{L}}$ with eigenvalue $\lambda = 0$, namely $\hat{\mathcal{L}}\hat{\rho}_{ss} = 0$. The dynamical properties depend on the non-zero complex eigenvalues. The Liouvillian gap $\bar{\lambda}$ is defined as the non-zero eigenvalue of $\hat{\mathcal{L}}$ with real part

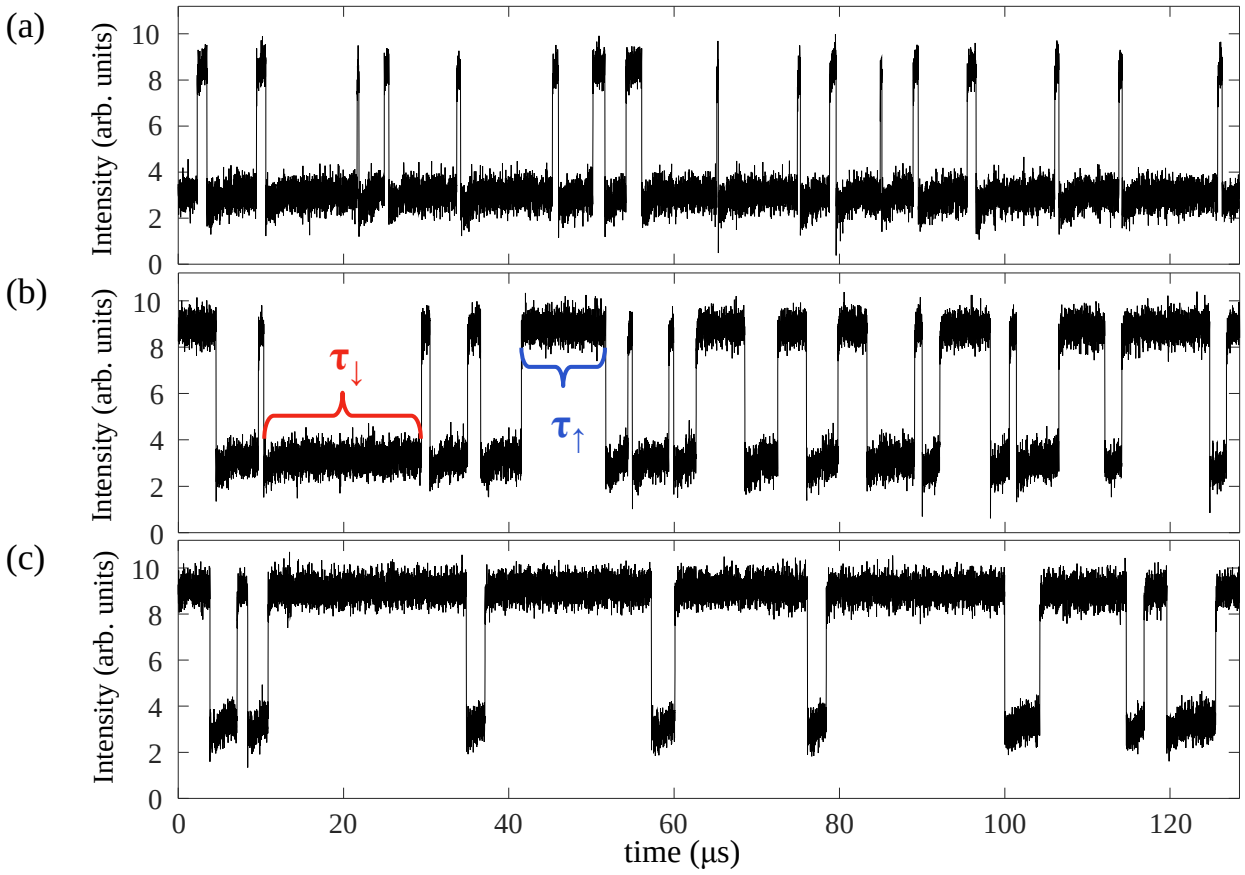

FIG. S2. Transmitted intensity as a function of time at a fixed driving power slightly below (a) and above (c) the center of the mean-field bistability. (b) is same as (a) and (c), but at a power close to the center of the mean-field bistability. The three panels show stochastic switching between two metastable states. Residence times in the lower and upper metastable states are labeled as $\tau_\downarrow$ and $\tau_\uparrow$, respectively.

closest to zero. In general, the Liouvillian gap becomes highly suppressed as a system enters a critical region [5]. This leads to a critical slowing down of the dynamics, and a dissipative phase transition when the gap $\bar{\lambda}$ closes. Around the bistability the imaginary part of $\bar{\lambda}$ is strictly zero and $|\mathrm{Re}\bar{\lambda}|$ exhibits a minimum at a driving intensity in the midst of the bistability region [6]. From the real part of $\bar{\lambda}$ the reaction time τ_R can be determined as: $\tau_R = 1/|\mathrm{Re}\bar{\lambda}|$. τ_R corresponds to the longest timescale on which the system relaxes to its steady-state. The transition point is defined as the intensity I_t where τ_R reaches the maximal value τ_{tunn}, the tunneling time.

A consequence of the above behavior of the Liouvillian gap is that the system can respond non-adiabatically when the driving power is varied across the optical bistability region. The sweep timescale τ_S is defined by the inverse normalised transition rate of the sweep (1): $\tau_S = |\dot{\epsilon}/\epsilon|^{-1}$, where ϵ is the distance from the transition point: $\epsilon = I(t) - I_t$. The non-adiabatic range is reached when the sweep timescale τ_S is smaller than the system reaction time τ_R, i.e. for $\tau_S < \tau_R$. If this condition is fulfilled, the system can not relax to its steady-state and a dynamic hysteresis arises. The point where the system enters or exits this non-adiabatic regime can be estimated by equating the two timescales: $\tau_S = \tau_R$. This allows to determine the size of the non-adiabatic range δI, as indicated by the blue dashed lines in the inset of Fig. 3(b) of the main manuscript for $U = 0.0075\gamma$ and $\Delta = \gamma$. Reference [6] showed that δI exhibits the same double power-law scaling as the hysteresis area. Moreover, in the slow sweep limit the prefactor of the power law with exponent -1 is directly related to the tunneling time: $\delta I = 2\tau_{\mathrm{tunn}} P_s/t_s$. The above scaling analysis was used to calculate the results in Fig. 3(b) and Fig. 4(b) of the main manuscript.

Comparing hysteresis measurements and non-adiabatic range calculations

A quantitative comparison between dynamic hysteresis measurements and non-adiabatic range calculations based on the scaling analysis described above requires a precise knowledge of the experimental excitation efficiency. This is needed to compare driving powers. Since excitation through the cryostat makes it difficult to know the excita-

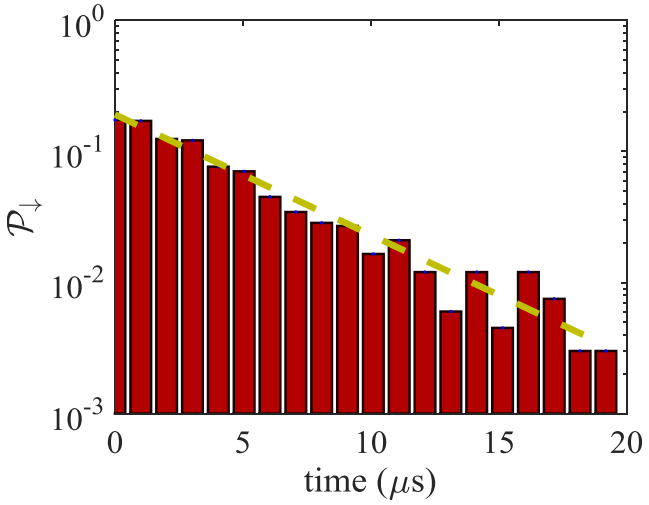

FIG. S3. Residence time distribution in the upper metastable state in Fig. S2(b). The distribution has been normalized such that the vertical axis corresponds to the probability for decay from the metastable state. The dashed line is a least-squares fit of an exponential function to the experimental data. The decay time retrieved from the fit is 4.7 ± 0.5 μs.

tion efficiency exactly, we deduced it by requiring that the theoretical range where the transition occurs in Fig. 1(c) of the main manuscript corresponds to the experimental one observed in Fig. 2(d). With this approach, we deduced a conversion factor of 0.75 between the theoretical units of γ^2 for the driving intensity and the experimentally measured power in μW, i.e.: $I[\gamma^2] = 0.75$ Power $[\mu W]$.

The values of U/γ used in the calculations in Fig. 3(b) and Fig. 4(b) of the main manuscript were adjusted with respect to the corresponding estimates for the experimental cavities (see above). For the calculations corresponding to cavity 1 and cavity 2, we took the experimentally estimated value of U/γ times a factor of 0.4 and 3.5, respectively. Note that the adjusted values are within the experimental uncertainties given above. These adjustments were only done to match the measured time of the transition to the power law with exponent -1, and they do not affect in any way the retrieved exponents. For cavity 3, the estimated $U/\gamma = 2^{+8}_{-1.6} \cdot 10^{-5}$ was replaced by the value $U/\gamma = 0.002$ in the calculations. This modification is due to the extremely small experimental value of U/γ being beyond our computational capabilities. Despite this seemingly large adjustment of U/γ , both experimental and theoretical curves follow a single power law within the observation window because fluctuations are largely irrelevant to the dynamics given the large average photon number in cavity 3.

In the caption of Fig. 4 we also mention that some of the curves were multiplied by a constant factor (given in the caption) simply for improving the clarity of the figure. These multiplications were only done to improve the visibility of details in the data given the finite space for the figure. These multiplications do not affect in any way the retrieved exponents, nor do they affect the critical times of the transition from one power law to another; they only shift the curves down or up in the log scale.

Finally, we would like to mention that a double power law decay of the hysteresis area could also be observed when a nonlinear system is subjected to thermal (or other) fluctuations. However, the exponents and critical times can depend on the details of the system. For instance, Luse and Zangwill calculated different exponents for several mean-field treatments of the kinetic Ising model [7]. In our optical experiments, where laser shot is the only relevant source of fluctuations, the measured exponents are in good agreement with calculations including quantum fluctuations only.

[1] H. Abbaspour, G. Sallen, S. Trebaol, F. Morier-Genoud, M. T. Portella-Oberli, and B. Deveaud, Phys. Rev. B **92**, 165303 (2015).
[2] S. Rodriguez *et al.*, Nature Commun. **7**, 11887 (2016).
[3] C. Ciuti, V. Savona, C. Piermarocchi, A. Quattropani, and P. Schwendimann, Phys. Rev. B **58**, 7926 (1998).
[4] H. Risken and K. Vogel, Phys. Rev. A **38**, 1349 (1988).
[5] E. M. Kessler, G. Giedke, A. Imamoglu, S. F. Yelin, M. D. Lukin, and J. I. Cirac, Phys. Rev. A **86**, 012116 (2012).
[6] W. Casteels, F. Storme, A. Le Boité, and C. Ciuti, Phys. Rev. A **93**, 033824 (2016).
[7] C. N. Luse and A. Zangwill, Phys. Rev. E **50**, 224 (1994).